NASA

Technical Memorandum 80603

Alternative Beam Efficiency Calculations for a Large-Aperture Multiple-Frequency Microwave Radiometer (LAMMR)

DECEMBER 1979

National Aeronautics and
Space Administration

Goddard Space Flight Center
Greenbelt, Maryland 20771

ALTERNATIVE BEAM EFFICIENCY CALCULATIONS FOR A LARGE-APERTURE MULTIPLE-FREQUENCY MICROWAVE RADIOMETER (LAMMR)

Richard F. Schmidt
NASA/Goddard Space Flight Center
Greenbelt, Maryland 20771

ABSTRACT

The fundamental definition of beam efficiency, given in terms of a far-field radiation pattern, is used to develop alternative definitions which improve accuracy, reduce the amount of calculation required, and isolate the separate factors composing beam efficiency. Well-known definitions of aperture efficiency are introduced successively to simplify the denominator of the fundamental definition. The superposition of complex-vector spillover and backscattered fields is examined, and beam efficiency analysis in terms of power patterns is carried out. An extension from single to dual-reflector geometries is included. It is noted that the alternative definitions are advantageous in the mathematical simulation of a radiometer system, and are not intended for the measurements discipline where fields have merged and therefore lost their identity.

CONTENTS

APPENDIXES

ILLUSTRATIONS

GLOSSARY OF NOTATION

η_B	beam efficiency
Ω_0	solid angle limit
$P(\Omega)$	power density distribution
$P_1(\Omega)$	power density distribution of far-field aperture-antenna pattern
$P_2(\Omega)$	power density distribution of a far-field spillover pattern
MP	main polarization
CP	cross polarization
η_{SO}	spillover efficiency
$P_i(P)$	power density incident on paraboloid
$P_{\not F}$	total feed power
K_x	x-directed aperture current magnitude
K_y	y-directed aperture current magnitude
ds	differential area of circular aperture
σ	radial distance in circular aperture
ζ	azimuthal angle in circular aperture
η_{POL}	polarization efficiency
η_A	aperture efficiency
D	antenna aperture diameter
λ	wavelength
θ	spherical net polar angle
ϕ	spherical net azimuthal angle
$P_1(0, 0)$	power density at $(\theta, \phi) = (0, 0)$
$\bar{K}_i$	complex aperture current (i = x, y, or z)
K_i	magnitude of $\bar{K}_i$
E	electric field (a complex number)

$P_i(H)$	power density incident on hyperboloid
$P_{3T}(H)$	total power spilled around hyperboloid
$P_{2T}(P)$	total power spilled around paraboloid
η_{AH}	amplitude distribution efficiency of aperture
η_{AP}	phase distribution efficiency of aperture
$(x + iy)$	complex representation of E_1
$(u + iv)$	complex representation of E_2
$(w + iz)$	complex representation of E_3
E_T	total field
AP	aperture (domain of integration)

ALTERNATIVE BEAM EFFICIENCY CALCULATIONS FOR A LARGE-APERTURE MULTIPLE-FREQUENCY MICROWAVE RADIOMETER (LAMMR)

INTRODUCTION

Antenna beam efficiency is defined in the literature as

$$\eta_B \doteq \frac{\iint_{\Omega_0} P(\Omega)\, d\Omega}{\iint_{4\pi} P(\Omega)\, d\Omega} \tag{1}$$

where $P(\Omega)$ denotes power density of the radiation pattern and Ω_0 is the solid-angle region associated with the main beam for which efficiency is evaluated (Ref. 1, p. 61). Frequently Ω_0 is the solid angle out to the first null of an idealized system. Sometimes Ω_0 is established via rules such as two and one-half times the half-power beamwidth for every azimuthal pattern cut considered. Other rules-of-thumb are encountered, some of which transcend the first null, etc.

In the definition given above there is a presumption that a radiation pattern per se exists, and no distinction is made with regard to "transmit" and "receive" patterns, ordinarily taken to be reciprocal. Subsequently the "transmit" point of view will be taken to develop the alternative definitions, by obtaining the separation of certain factors, even though the LAMMR is a passive sensor. Also, it will not be assumed that the pattern per se exists; the elements which eventually comprise that pattern will be introduced explicitly instead.

An inspection of the numerator

$$\iint_{\Omega_0} P(\Omega)\, d\Omega \tag{2}$$

where $P(\Omega)$ is the power density of the radiation pattern, allows the conclusion that two orthogonal polarization states are to be integrated over angle Ω_0 of the main beam. For an instrument intended to be responsive to a single linear state, however, it can be argued that any cross-polarization should be charged against the value of beam efficiency by integrating over only the

main polarization component in the numerator. The cross-polarization effect is usually small for reasonably flat reflectors and is a function of the f number or ratio of focal length to diameter (F/D).

Finally, the existing literature suggests that alternatives to the fundamental definition might be advantageous (Ref. 1, p. 61). Introduction of the definition of directive gain has the immediate consequence of eliminating the denominator of the original definition. The denominator,

$$\iint_{4\pi} P(\Omega)\, d\Omega \quad , \tag{3}$$

is difficult to simulate mathematically with accuracy over 4π solid angle with most algorithms used to calculate the field values. Further, the cost of such mathematical simulations may be excessive, particularly for apertures which are electrically large. (Some discussion of this problem can be found in APPENDIX-E.) The introduction of aperture efficiency (η_A) then motivates a search for the explicit introduction of other "efficiency" factors, particularly spillover efficiency (η_{SO}).

BEAM EFFICIENCY (SINGLE REFLECTOR SYSTEMS)

The fundamental definition of beam efficiency, (1), is now rewritten in terms of power as follows,

$$\eta_B = \frac{\iint_{\Omega_0} P_{1_{MP}}(\Omega)\, d\Omega + \iint_{\Omega_0} P_{2_{MP}}(\Omega)\, d\Omega}{\iint_{4\pi} [P_{1_{MP}}(\Omega) + P_{1_{CP}}(\Omega) + P_{2_{MP}}(\Omega) + P_{2_{CP}}(\Omega)]\, d\Omega} \tag{4}$$

where $P_1(\Omega)$ refers to the far-field forward and backward scattered power pattern from the offset paraboloid and $P_2(\Omega)$ refers to the spillover power pattern. Main and cross-polarization components (MP, CP) are distinguished here. The spillover power pattern differs from the prime-feed power pattern in that the former is taken to be zero inside the paraboloidal reflector geometrical bounds as viewed from the feed phase center.

Even though the complex fields of the spillover pattern superimpose with those of the calculated scattered pattern and lose their identity in the physical world, the summation of power indicated above can be justified in mathematical simulation of the radiometer (Ref. 2). See APPENDIX-A.

From Figure A-1 it can be seen that spillover efficiency,

$$\eta_{SO} = \frac{\iint_{4\pi} [P_{1_{MP}}(\Omega) + P_{1_{CP}}(\Omega)]\, d\Omega}{\iint_{4\pi} [P_{1_{MP}}(\Omega) + P_{1_{CP}}(\Omega) + P_{2_{MP}}(\Omega) + P_{2_{CP}}(\Omega)]\, d\Omega} \tag{5}$$

$$= \frac{P_i(P)}{P_{\mathcal{F}}} = \frac{\text{(power incident on } \gamma_P)}{\text{(total feed power)}} ,$$

can be evaluated in terms of the feed characteristics and geometric bounds alone.

Then, neglecting a low-intensity feed pattern term in equation (4),

$$\boxed{\eta_B = \frac{\eta_{SO} \iint_{\Omega_0} P_{1_{MP}}(\Omega)\, d\Omega}{\iint_{4\pi} [P_{1_{MP}}(\Omega) + P_{1_{CP}}(\Omega)]\, d\Omega}} \tag{6}$$

But an approximation to polarization efficiency over 4π can be made at high frequencies in terms of orthogonal aperture currents K_x and K_y associated with the 2π backscatter half-space of the main aperture by

$$\eta_{POL} = \frac{\iint_{4\pi} P_{1_{MP}}(\Omega)\, d\Omega}{\iint_{4\pi} [P_{1_{MP}}(\Omega) + P_{1_{CP}}(\Omega)]\, d\Omega} = \frac{\iint_{AP} K_x^2\, ds}{\iint_{AP} (K_x^2 + K_y^2)\, ds} \tag{7}$$

where K_x refers to MP and K_y refers to CP arbitrarily. Here, the differential aperture area of the radiometer,

$$ds = \sigma \, d\zeta \, d\sigma \quad , \tag{8}$$

is given in terms of local radial and azimuthal aperture variables, σ and ζ, respectively.

Once again, the far-field radiation patterns are avoided, and beam efficiency becomes

$$\eta_B = \eta_{SO} \, \eta_{POL} \frac{\iint_{\Omega_0} P_{1_{MP}}(\Omega) \, d\Omega}{\iint_{4\pi} P_{1_{MP}}(\Omega) \, d\Omega} \tag{9}$$

But aperture efficiency in terms of the physical reflector diameter (D) and wavelength (λ) is defined as

$$\eta_A = \frac{P_{1_{MP}}(0, 0)}{\frac{1}{4\pi} \left(\frac{\pi D}{\lambda}\right)^2 \iint_{4\pi} P_{1_{MP}}(\Omega) \, d\Omega} \tag{10}$$

where

$$P_{1_{MP}}(\theta, \phi) = P_{1_{MP}}(0, 0) \tag{11}$$

is the beam-axis power density. Now aperture efficiency can also be calculated without involving the far-field radiation pattern characteristics (Ref. 3).

Before detailing the actual form of the aperture efficiency calculations it is noted that this coefficient is a measure of effectiveness (directive gain) for complex fields, initially, which have actually impinged on a reflector surface and is therefore unrelated to spillover fields. That is, an aperture distribution can be postulated, or computed, and aperture efficiency can be evaluated entirely in terms of aperture current distribution.

Aperture efficiency should be generalized for the present discussion as the product of amplitude-distribution efficiency times phase-distribution efficiency, particularly in view of the fact that system distortion due to mechanical rotation (1 rps) and solar loading will affect aperture phase. An equivalent complex distribution can also be defined (Ref. 3). For confocal optics and undistorted reflectors the definition of aperture efficiency in the real domain, above, is adequate.

In any event, the generalization to the complex domain is easily achieved. Avoidance of the far-field radiation patterns in these calculations is the principal objective since few, if any, diffraction algorithms are very reliable over 4π solid angle, and economic considerations (computer cpu-time) also indicate that an alternative based on the fundamental definition of beam efficiency should be implemented. (APPENDIX-E shows that a departure from the alternative approach developed in this document is sometimes possible.)

Then, introducing aperture efficiency,

$$\eta_B = \frac{\eta_{SO}\ \eta_{POL}\ \eta_A \left(\frac{\pi D}{\lambda}\right)^2 \iint_{\Omega_0} P_{1_{MP}}(\Omega)\ d\Omega}{4\pi\ P_{MP}(0,\ 0)} \tag{12}$$

For convenience, the integral forms of Reference 3 are given here for computing amplitude and phase aperture efficiency in terms of currents rather than the far-field radiation pattern.

$$\eta_{AM} = \frac{[\iint_{AP} K_i(\sigma, \zeta)\ ds / \iint_{AP} ds]^2}{\iint_{AP} K_i^2(\sigma, \zeta)\ ds / \iint_{AP} ds}\ , \tag{13}$$

$$\eta_{AP} = \frac{|\iint_{AP} \bar{K}_i(\sigma, \zeta)\ ds\ |^2}{(\iint_{AP} |\bar{K}_i(\sigma, \zeta)|\ ds)^2}\ , \tag{14}$$

where $\eta_A = \eta_{AM}\,\eta_{AP}$ is easily proved for the general case. In the above, $\bar{K}_i$ is the complex main-polarization current component, projected into the aperture plane and

$$|\bar{K}_i| = K_i\ . \tag{15}$$

Furthermore, it is possible to employ similar definitions which are cast in terms of the feed-angle variables (Θ, Φ) and are more convenient to use when functional forms rather than feed data

are assumed for feed representations. The equations for η_{AM} and η_{AP} are formidable in appearance, but the evaluation process is committed to an auxilliary computer program and can be carried out in an effective manner.

From (12) it can be seen that the alternative means for computing beam efficiency for a single reflector relies on feed characteristics ($\mathcal{F}$) and geometric bounds (Ω_0), and aperture and polarization efficiency calculations in the aperture plane. Far-field radiation pattern integration is restricted to the vicinity of the main beam (Ω_0), which is both accurate and inexpensive in terms of computer cpu time. This approach should be contrasted with (1), the fundamental definition, which requires an accurate evaluation of $P_{1_{MP}}(\Omega)$ and $P_{1_{CP}}(\Omega)$ over 4π solid-angle for a nominal 4-meter aperture in the frequency range 1.4 GHz to 91.0 GHz.

BEAM EFFICIENCY (DUAL REFLECTOR SYSTEMS)

The extension of the definition of beam efficiency from a single offset paraboloidal reflector to a dual offset (Cassegrain) system appears to be straightforward. The fundamental expression, (1), is reformed as

$$\eta_B = \frac{\iint_{\Omega_0} P_{1_{MP}}(\Omega)\, d\Omega + \iint_{\Omega_0} P_{2_{MP}}(\Omega)\, d\Omega + \iint_{\Omega_0} P_{3_{MP}}(\Omega)\, d\Omega}{\iint_{4\pi} [P_{1_{MP}}(\Omega) + P_{1_{CP}}(\Omega) + P_{2_{MP}}(\Omega) + P_{2_{CP}}(\Omega) + P_{3_{MP}}(\Omega) + P_{3_{CP}}(\Omega)]\, d\Omega} \qquad (16)$$

where $P_2(\Omega)$ and $P_3(\Omega)$ denote spillover power patterns associated with a virtual point source and a physical feed, respectively. See Figure B-1 of APPENDIX B. Main and cross-polarization components are distinguished here. The spillover patterns differ from the virtual point source and physical feed patterns in that the spillover patterns are taken to be zero where radiation is intercepted by reflector surfaces. In passing it is noted that the primary feed pattern, ordinarily situated at the conjugate focus (F*) for Cassegrain systems, is intercepted by both the hyperboloid and the paraboloid geometrical bounds as viewed from F*.

Addition of power, rather than the superposition of complex-vector fields is justified as for the single reflector system and it is easily shown that the superposition of the three main-polarized feeds leads to

$$E_{1_{MP}}^2(\Omega) + E_{2_{MP}}^2(\Omega) + E_{3_{MP}}^2(\Omega) + E_1 E_{2_{MP}}^* + E_1^* E_{2_{MP}} + E_2 E_{3_{MP}}^* + E_2^* E_{3_{MP}} + E_3 E_{1_{MP}}^* + E_3^* E_{1_{MP}} \qquad (17)$$

where all mixed products involving E_1 or E_1^* may be set to zero due to their oscillatory nature.

The terms $E_2E_3^*$ and $E_2^*E_3$ (cross-correlations) relating to the radiation patterns of a virtual point source (E_2) and a physical feed (E_3) are viewed as follows. Neither of E_2 or E_3 is as oscillatory as E_1, and the periodicity of E_2 and E_3 is about equal. From Figure B-1 it can be seen that the highest values of E_2 are spatially uncorrelated with the highest values of E_3, leading to a zero product. The lower values of E_2 and E_3 may be completely correlated spatially, but their products will approach zero because their values are both extremely low. Only the self-correlations $E_{1_{MP}}^2(\Omega)$, $E_{2_{MP}}^2(\Omega)$, and $E_{3_{MP}}^2(\Omega)$ remain, and are proportional to $P_{1_{MP}}(\Omega)$, $P_{2_{MP}}(\Omega)$, and $P_{3_{MP}}(\Omega)$ respectively. See APPENDIX-B for background.

An identical argument can be made for the cross-polarization components of the field spilled over the reflectors.

Since

$$\eta_{SO} = \frac{\iint_{4\pi} [P_{1_{MP}}(\Omega) + P_{1_{CP}}(\Omega)]\, d\Omega}{\iint_{4\pi} [P_{1_{MP}}(\Omega) + P_{1_{CP}}(\Omega) + P_{2_{MP}}(\Omega) + P_{2_{CP}}(\Omega) + P_{3_{MP}}(\Omega) + P_{3_{CP}}(\Omega)]\, d\Omega} \qquad (18)$$

it follows that, upon neglecting low-intensity real and virtual feed pattern terms in equation (16),

$$\eta_B = \frac{\eta_{SO}(H)\, \eta_{SO}(P)\, \eta_{POL}\, \eta_A \left(\frac{\pi D}{\lambda}\right)^2 \iint_{\Omega_0} P_{1_{MP}}(\Omega)\, d\Omega}{4\pi\, P_{1_{MP}}(0, 0)} \qquad (19)$$

since

$$\eta_{SO} = \eta_{SO}(H)\,\eta_{SO}(P) = \frac{P_i(H)}{P_i(H) + P_{3T}(H)} \cdot \frac{P_i(P)}{P_i(P) + P_{2T}(P)} = \frac{P_i(P)}{P_{\mathscr{T}}} . \qquad (20)$$

Here $\eta_A = \eta_{AM}\ \eta_{AP}$, as before.

CONCLUSION

The prospect of obtaining an accurate and economical numerical solution for beam efficiency via the fundamental equation,

$$\boxed{\eta_B = \frac{\iint_{\Omega_0} P(\Omega)\, d\Omega}{\iint_{4\pi} P(\Omega)\, d\Omega}} \quad , \qquad (1)$$

is such that an alternative formulation may be necessary. This document suggests that the following factors may be computed by means of separate subroutines:

$\eta_{SO}(H)$	in physical 3-space
$\eta_{SO}(P)$	in physical 3-space
η_{AM}	in the aperture plane
η_{AP}	in the aperture plane
η_{POL}	in the aperture plane

All of these are well-defined and do not involve diffraction analysis (physical optics solutions). Assuming that the foregoing have been computed, the beam-efficiency of a dual-reflector large-aperture antenna is obtained from an alternate form:

$$\boxed{\eta_B = \frac{\eta_{SO}(H)\,\eta_{SO}(P)\,\eta_{POL}\,\eta_{AM}\,\eta_{AP}\left(\frac{\pi D}{\lambda}\right)^2}{4\pi\, P_{1\,MP}(0,0)} \iint_{\Omega_0} P_{1\,MP}(\Omega)\, d\Omega} \qquad (21)$$

Here the only radiation pattern integration is over a well-defined main beam. Dimensional requirements are satisfied and normalization is achieved via the axial value $P_{1\,MP}(0, 0)$ of the main beam. The factors which affect beam efficiency are explicitly identified.

The preceding development has tacitly assumed a well-defined, deterministic surface. In practice the RMS phase errors associated with the aperture constitute a primary limitation on the antenna efficiency, and a multiplicative gain degradation factor is applied to η_B, above.

$$\eta_{RMS} = e^{-(2\pi\delta/\lambda)^2} \tag{22}$$

Here (δ) is the RMS phase front displacement from planar, taken over the aperture, in a set of units consistent with that chosen for wavelength.

APPENDIX-C is included to substantiate the conclusions reached by the independent derivations of this document, particularly with regard to the factors η_A and η_{SO}. Comparisons are made with equations found in Ref. 4, p. 218.

APPENDIX-D is included to form an appreciation of the factor

$$F = \frac{\left(\frac{\pi D}{\lambda}\right)^2 \iint_{\Omega_0} P_{1_{MP}}(\Omega)\, d\Omega}{4\pi\, P_{1_{MP}}(0,0)} , \tag{23}$$

which is multiplied against the associated efficiency factor

$$H = \eta_{SO}(H)\, \eta_{SO}(P)\, \eta_{POL}\, \eta_{AM}\, \eta_{AP} \tag{24}$$

and to detail some of the practical aspects of the evaluation of beam efficiency (η_B) when the algorithm used to form the diffraction pattern cannot be relied upon at the larger polar angles.

APPENDIX-E is included to illustrate a hybrid approach for obtaining beam efficiency.

APPENDIX-F is included since it is a simple method for arriving at beam efficiency predicated on equations (4) or (16).

ACKNOWLEDGMENTS

The author acknowledges discussions with Dr. J. Eckerman and Mr. J. L. King on the topic of beam efficiency calculations. In addition, the author acknowledges the contributions of Mr. R. Miezis (Sigma Data Services Corp.) and Mr. L. R. Dod, GSFC, who provided material cited in this document and elaborated on details of specific approaches used in industry. The material on beam efficiency via the hybrid and feed integration techniques was motivated by discussions with Dr. J. Fujioka (Aerojet Electrosystems Company). Thanks are also due to the numerous reviewers of this document, particularly Mr. L. R. Dod, Mr. P. Shu, Dr. J. Shiue, Mr. R. Weber, Mr. R. Miezis, Ms. J. Wolf (SDSC), and Mr. K. Green (Microwave Research Corporation), who went into the controversial aspects of the material and gave most generously of their time.

REFERENCES

1. Rusch, W. V. T., and Potter, P. D., "Analysis of Reflector Antennas," Academic Press, 1970.

2. Hughes Aircraft Company, "Geosynchronous Microwave Atmospheric Sounding Radiometer (MASR) Antenna Feasibility Study," Final Report, Contract NAS-5-24087, Vol. III, Hughes Ref. No. D9 236, pp. 77-569, Jan. 1978.

3. Schmidt, R. F. and Bartley, W. K., "Antenna Illumination-Distribution Efficiency", Goddard Space Flight Center X-811-76-73, May 1976.

4. Kraus, J. D., "Radio Astronomy," McGraw-Hill Book Company," 1966.

5. Kraus, J. D., "Antennas", McGraw-Hill Book Company, 1950.

6. Skolnik, M. I., "Radar Handbook", McGraw-Hill Book Company, 1970.

7. Born, M. and Wolf, E., "Principles of Optics", Pergamon Press, 1964.

8. General Electric (Space Division), "Design Study – High Resolution Microwave Images (HRMI), Final Report, Contract NAS-5-23412, Modification No. 134.

APPENDIX A
SINGLE REFLECTOR – SPILLOVER SUPERPOSITION

Consider the main polarization component of field spilled over the rim of a paraboloid as shown in Figure A-1. Superimposing this field with the corresponding scattered field in the complex (i) domain,

$$\begin{aligned} E_{\substack{T \\ MP}} &= E_{1_{MP}}(\Omega) + E_{2_{MP}}(\Omega) \\ &= (x + iy) + (u + iv) \\ &= (x + u) + i(y + v) \end{aligned} \tag{1-A}$$

Form $E^2_{\substack{T \\ MP}} \doteq 0$ where

$$i(yu - xv) + i(xv - yu) = 0 \quad . \tag{2-A}$$

Then

$$E^2_{\substack{T \\ MP}} = E_1^2 + E_2^2 + E_1 E_2^* + E_1^* E_2 \approx E_1^2 + E_2^2 \; \alpha \; P_{\substack{1 \\ MP}} + P_{\substack{2 \\ MP}} \tag{3-A}$$

due to the oscillatory nature of the scattered field (E_1) of the high gain radiation pattern of the main aperture. The cross-correlations involving conjugate factors do not appear to have a physical interpretation as do the self-correlations.

A identical argument can be made for the cross-polarization components of the fields spilled over the reflector.

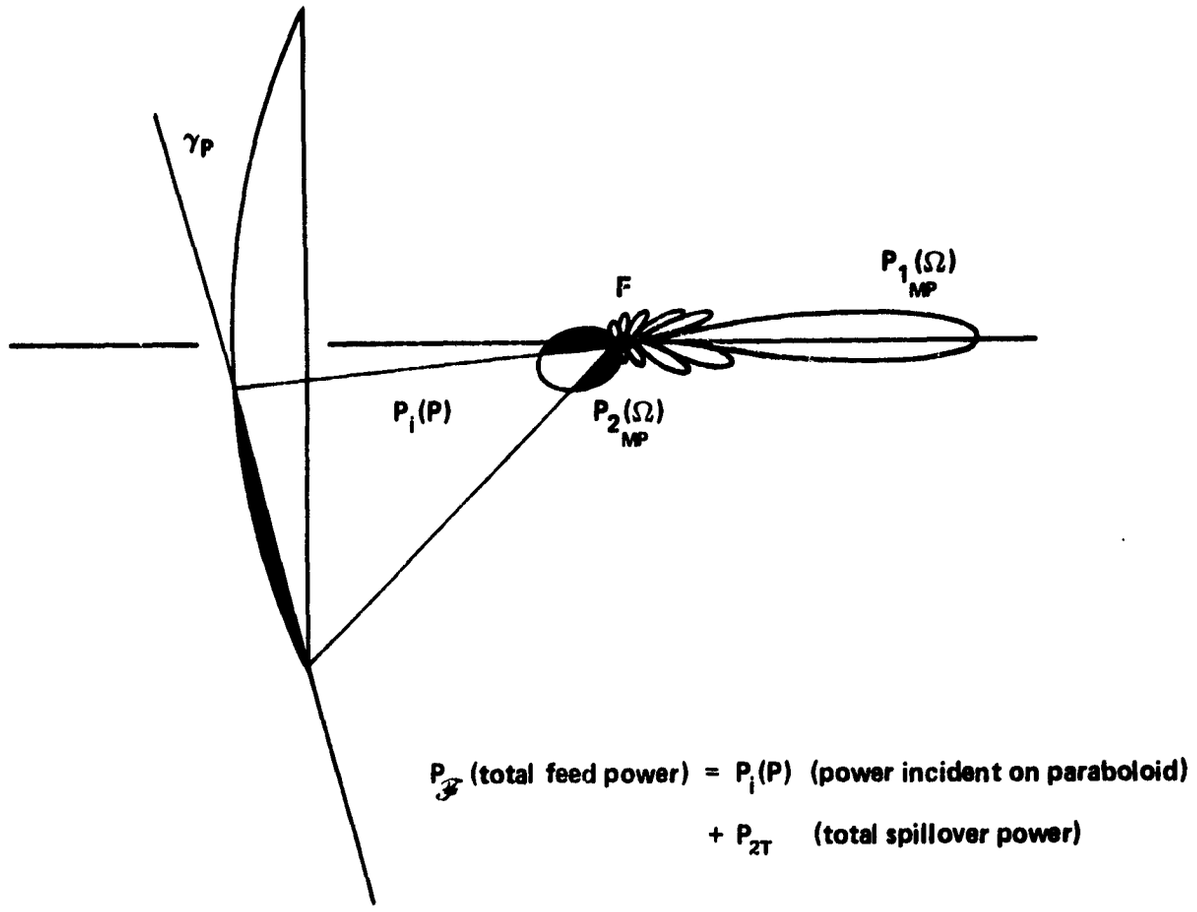

Figure A-1. Single Offset Reflector Geometry.

APPENDIX B
DUAL REFLECTOR – SPILLOVER SUPERPOSITION

Consider the main polarization components of field spilled over the rims of the hyperboloidal subreflector and paraboloidal main reflector as suggested by Figure B-1. Assume a non-trivial superposition of the spillover fields E_2 and E_3 onto the main reflector scattered field E_1 in the complex (i) domain

$$\begin{aligned} \underset{MP}{E_1} &= E_1(\Omega) + \underset{MP}{E_2}(\Omega) + \underset{MP}{E_3}(\Omega) \\ &= (x + iy) + (u + iv) + (w + iz) \\ &= (x + u + w) + i(y + v + z) \end{aligned} \tag{1-B}$$

Form $\underset{MP}{E_T^2} + 0$ where

$$i(yu - xv) + i(xv - yu) + i(vw - uz) + i(uz - vw) + i(zx - wy) + i(wy - xz) = 0 . \tag{2-B}$$

Then

$$\begin{aligned} \underset{MP}{E_T^2} &= E_1^2 + E_2^2 + E_3^2 + E_1E_2^* + E_1^*E_2 + E_2E_3^* + E_2^*E_3 + E_3E_1^* + E_3^*E_1 \\ &\approx E_1^2 + E_2^2 + E_3^2 \propto \underset{MP}{P_1} + \underset{MP}{P_2} + \underset{MP}{P_3} \end{aligned} \tag{3-B}$$

due to either the oscillatory nature of the scattered field (E_1) of the high-gain radiation pattern of the main aperture, the spatially uncorrelated nature of the higher levels of the spillover fields E_2 and E_3, or the low levels of the spillover fields when they are spatially correlated.

An identical argument can be made for the cross-polarization components of the fields spilled over the reflectors.

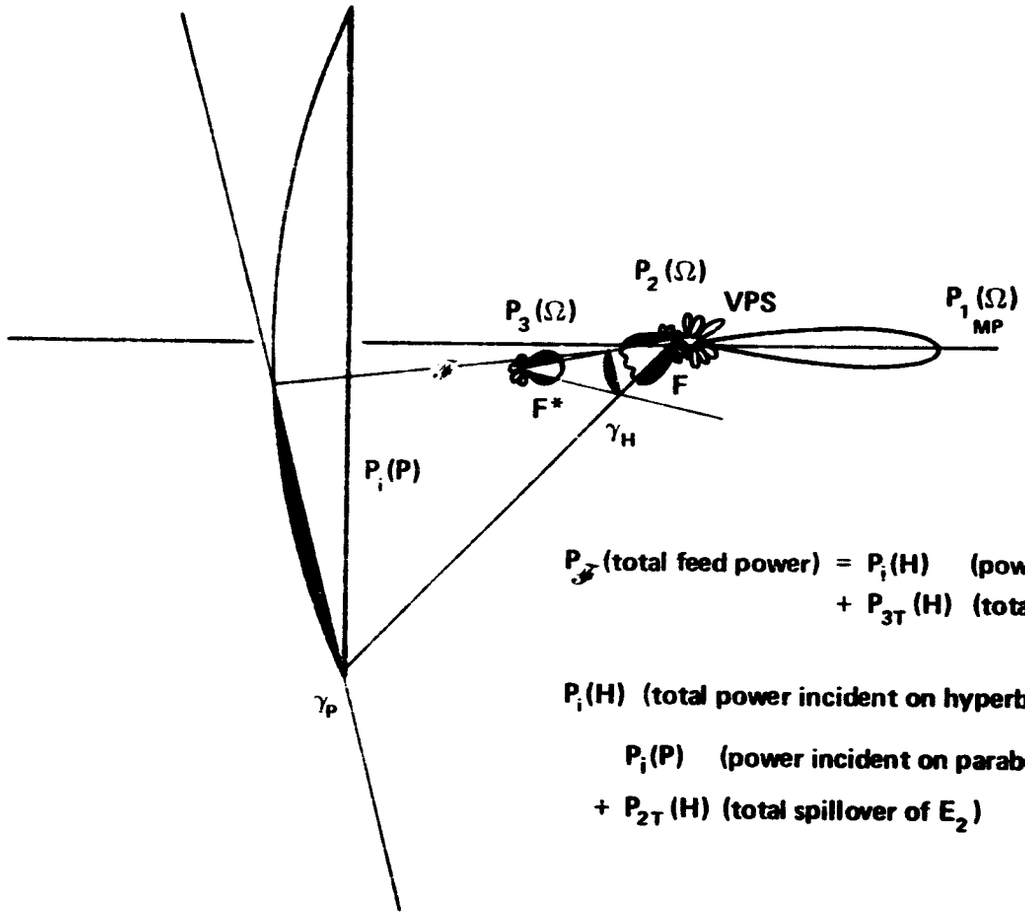

P_T (total feed power) = $P_i(H)$ (power incident on hyperbaloid)
+ $P_{3T}(H)$ (total spillover of E_3)

$P_i(H)$ (total power incident on hyperboloid) =

$P_i(P)$ (power incident on paraboloid)

+ $P_{2T}(H)$ (total spillover of E_2)

Figure B–1. Dual–Offset Reflector Geometry.

APPENDIX D
ALTERNATIVE FORMS

Reference 4 implicitly contains alternative forms for beam efficiency which parallel those of this document with respect to aperture and spillover efficiency. The isolation of the factor (η_A), previously identified in Ref. 1, appears in the expression

$$\boxed{\frac{\eta_A}{\eta_B} = \frac{\lambda^2}{Ap\ \Omega_M}} \tag{1-C}$$

where

$$Ap = \pi(D/2)^2 = \text{aperture area,}$$

and

$$\Omega_M = \iint_{\Omega_0} P_n(\theta, \phi)\, d\Omega = \iint_{\Omega_0} \frac{P_1(\theta,\phi)\, d\Omega}{P_1(0,0)} = \iint_{\Omega_0} \frac{P_1(\Omega)\, d\Omega}{P_1(0,0)} =$$

main-beam solid-angle, Ref. 4, p. 159. (2-C)

It can be seen that it is possible to rewrite the ratio of aperture efficiency to beam efficiency, given above, as

$$\eta_B = \eta_A \frac{(\pi D/\lambda)^2}{4\pi} \iint_{\Omega_0} \frac{P_1(\Omega)\, d\Omega}{P_1(0,0)} \tag{3-C}$$

which agrees with the form of η_B given previously.

The isolation of factor (η_{SO}), not previously associated with any reference in this development, is via the expression

$$\boxed{\epsilon_f = \frac{\iint_{\Omega_R} P_{\mathscr{F}}\, d\Omega}{\iint_{4\pi} P_{\mathscr{F}}\, d\Omega} \equiv \eta_{SO}} \quad , \tag{4-C}$$

where (P_{ψ}) is the power-pattern of the feed, and (Ω_R) is the solid angle subtended by a reflector as viewed from the feed point (Ref. 4, p. 220). The factor (ϵ_f) is termed "feed-efficiency" in the cited reference, and is recognized as being identical with spillover efficiency (η_{SO}).

It is noted that the spillover and aperture efficiencies were generalized in this document, the former to dual-reflector systems, and the latter to complex aperture efficiency. The isolation of both of these factors has been suggested previously in Ref. 4, at least implicitly. Kraus retains the integral over 4π solid-angle as it originally appears in the fundamental definition of beam efficiency, probably because he was dealing with experimentally derived radiation patterns and was not computing $P_1(\Omega)$. In the present document aperture efficiency (η_A) appears explicitly, and an expensive and inaccurate numerical double integral is avoided. At this writing polarization efficiency has not been found in the literature by the author as an explicit factor in the definition of beam efficiency.

APPENDIX D
BEAM EFFICIENCY CALCULATIONS (ALTERNATIVE METHOD)

Assume that the alternative form of beam efficiency presented in the conclusion of this document,

$$\eta_B = HF \quad , \tag{1-D}$$

is to be used, Suppose that the polarization and aperture phase-distribution efficiencies of a single-reflector configuration are

$$\eta_{POL} = \eta_{AP} \approx 1.0 \quad , \tag{2-D}$$

and the spillover and aperture amplitude-distribution efficiencies are

$$\eta_{SO} = \eta_{AM} \approx 0.90 \tag{3-D}$$

It follows that

$$\boxed{\eta_B \approx 0.81F} \tag{4-D}$$

for this example. What value of beam efficiency can be obtained under these assumptions? This is of particular interest to LAMMR. Can $\eta_B \approx 0.90$ be achieved?

An approximate evaluation of the factor (F) can be carried out in a relatively simple way. Since

$$F = \frac{\left(\frac{\pi D}{\lambda}\right)^2}{4\pi} \quad \frac{\iint_{\Omega_0} P_{1_{MP}}(\Omega)\ d\Omega}{P_{1_{MP}}(0,0)} \quad , \tag{5-D}$$

the only difficulty is with the integral. The beamwidth-squared for the assumed aperture efficiency is approximately

$$\left(\frac{BW_{-3\,dB}}{rad.^2}\right)^2 = \left[\left(\frac{70\lambda}{D}\right)\left(\frac{\pi}{180}\right)\right]^2 = \theta_1^2 = \Omega_M = \frac{\iint_{\Omega_0} P_{1_{MP}}(\Omega)\, d\Omega}{P_{1_{MP}}(0,0)} \quad , \qquad (6\text{-D})$$

θ_1^2: rad.^{2}; Ω_M: rad.^{2}

so that

$$F = \frac{\pi^3}{4}\left(\frac{7}{18}\right)^2 \approx 1.17 \quad , \qquad (7\text{-D})$$

which results, initially, in a beam efficiency of about 0.95 for the conditions indicated. Ref. 4, p. 159; Ref. 5, p. 25. Numerical integration over solid angle (Ω_0) of the computed main beam pattern is anticipated in more general cases. The preceding is to establish $F > 1$.

It is noted that the beamwidth formula used above is for a 10 dB illumination distribution edge-taper, and this is reasonable in view of the aperture efficiency of 0.90 used in these calculations. For example, a Gaussian current distribution

$$K_i = K_0\, e^{-\alpha(\sigma/\sigma_2)^2} \qquad (8\text{-D})$$

with

$$\alpha = 1.15129 \qquad (9\text{-D})$$

leads to an edge-taper of 10 dB at $\sigma = \sigma_2$, and an amplitude distribution efficiency

$$\eta_{AM} = \frac{2(1 - e^{-\alpha})^2}{\alpha(1 - e^{-2\alpha})} = 0.90 \qquad (10\text{-D})$$

See Ref. 3, p. C-2.

A comparison is now made between the polar half-power beamwidth angle (θ_1), and a polar angle (θ_M) associated with the beam area (Ω_M), which is a solid angle. Circular or axial symmetry is assumed. See Figure D-1.

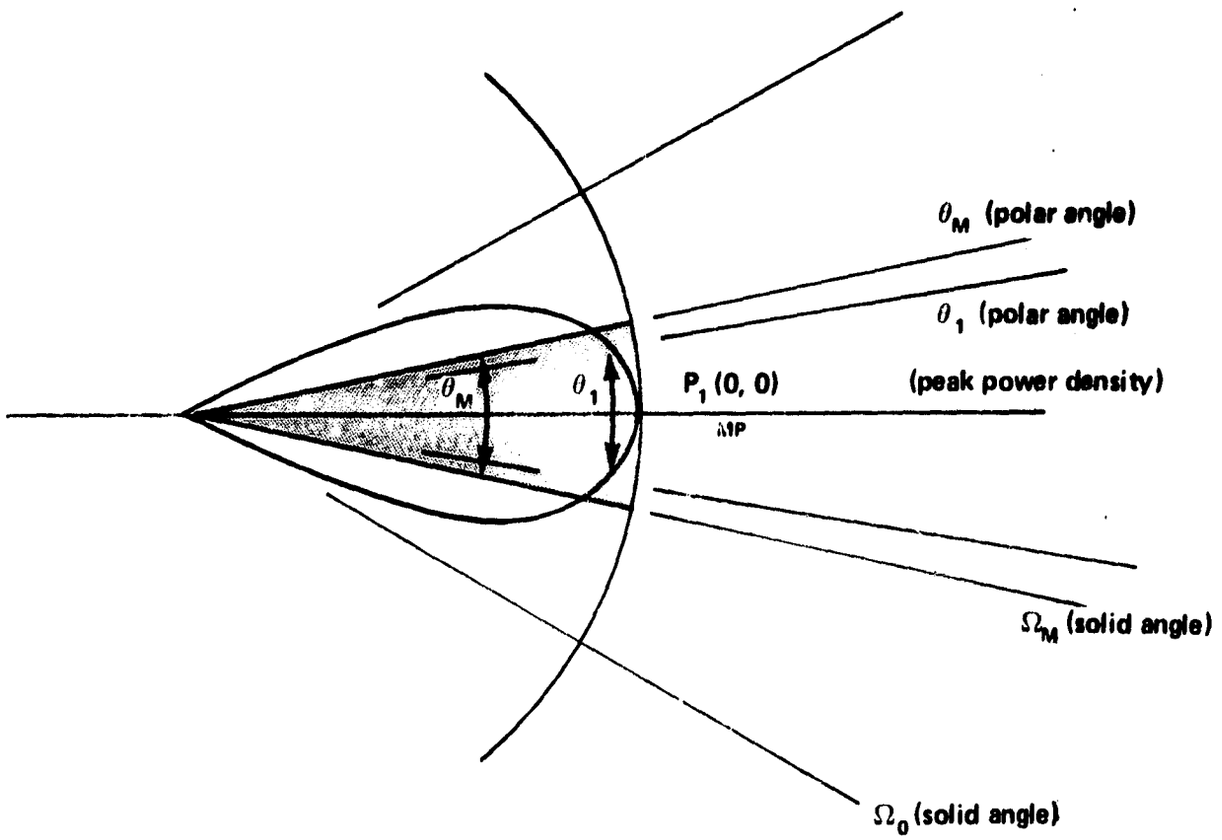

Figure D-1. Beam Width (θ_1) and Beam Area (Ω_M).

The power of the main beam, contained within the solid angle Ω_0 corresponding to the first null of a diffraction pattern, equals the power contained within the solid angle Ω_M assuming the power density throughout the latter equals the peak density value $P_1(0, 0)$. That is,

$$P_{1_{MP}}(0,0)\ \Omega_M = \iint_{\Omega_0} P_{1_{MP}}(\Omega)\, d\Omega = \int_{\phi=0}^{2\pi}\int_{\theta=0}^{\theta_M/2} P_{1_{MP}}(0,0)\, \sin\theta\, d\theta\, d\varphi \qquad (11\text{-D})$$

Then

$$\Omega_M = \theta_1^2 = 2\pi\,(-\cos\theta)\Big|_0^{\theta_M/2} = 2\pi\,(1 - \cos\theta_M/2), \qquad (12\text{-D})$$

or

$$\boxed{\cos\frac{\theta_M}{2} = 1 - \frac{\Omega_M}{2\pi} = 1 - \frac{\theta_1^2}{2\pi}} \qquad (13\text{-D})$$

For example, if θ_1 = 1 degree, θ_M = 1.13 degree, as suggested by Figure D-1. It is noted that both θ_1 and θ_M are double angles in the present discussion. The definition of solid angle (Ω_M) in terms of beamwidth (θ_1) is responsible for the inequality $\theta_M > \theta_1$. Figure D-2 illustrates this result graphically.

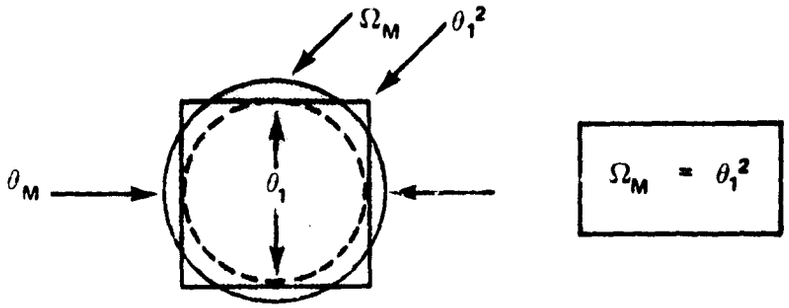

Figure D-2. Beam Width (θ_1) and Angle (θ_M) of Beam Area (Ω_M).

A review of the factor (η_{AM} F) of the preceding calculation was made at the suggestion of K. Green (MRC). Combining Equations (10) and (5-D) results in

$$\eta_{AM} F = \frac{\iint_{\Omega 0} P_{1\,MP}(\Omega)\, d\Omega}{\iint_{4\pi} P_{1\,MP}(\Omega)\, d\Omega} < 1 \qquad (7\text{-D})$$

Previously, it was assumed for the numerical example that

$$\eta_{AM} = 0.90 \quad ,$$

and then

$$F = 1.17$$

was obtained via Kraus' approximation formula. A 10dB edge-taper case was analyzed. But this results in a product

$$\eta_{AM} F = 1.05 > 1 \quad ,$$

which is impossible, indicating that the evaluation of (F) was imprecise. See Equation (7-D).

An independent second approach is now made via the equations of Reference 8. An aperture current distribution of the form

$$K = A + (1-A)\,[1-(\sigma/\sigma_{max})^2]^p \qquad (8\text{-D})$$

evaluated at $\sigma = 0$ and $\sigma = \sigma_{max}$ gives a ratio of central to edge current values of

$$\frac{K_1}{K_2} = \frac{1}{A} \qquad (9\text{-D})$$

The assumed edge-taper of -10dB is realized when

$$10\text{dB} = 10 \log_{10} \left(\frac{1}{A}\right)^2 \quad , \qquad (10\text{-D})$$

or

$$A = 0.316 \qquad (11\text{-D})$$

A computer program utilizing an analytical result of Ref. 8 and written by R. Miezis (SDSC), was then used to determine that

$$\eta_{AM} F = \frac{\iint_{\Omega 0} P_1(\Omega)\, d\Omega}{\iint_{4\pi} P_1(\Omega)\, d\Omega} \approx 0.955 < 1 \quad , \qquad (12\text{-D})$$

corresponding to the above value of A and p = 1. Then

$$F \approx \frac{0.955}{.90} = 1.06 > 1 \qquad (13\text{-D})$$

instead of $F \approx 1.17$, obtained previously. It is noted that $F > 1$ is still a conclusion, but

$$\eta_B = 0.81\ F = (0.81)\ (1.06) \approx 0.86 \qquad (14\text{-D})$$

instead of $\eta_B = 0.95$, obtained previously.

The discrepancy could be due to use of the approximation formula for beam area,

$$\Omega_M = \theta_1^2 \quad , \qquad (15\text{-D})$$

and/or use of the approximation formula for half power beamwidth,

$$BW_{-3dB} = \frac{70^{\lambda}}{D}$$

for an edge-taper of 10dB. In practice, the main-beam energy is obtained by numerical methods and a proven computer program, rather than by either approximation method presented here to arrive at factor (F).

APPENDIX E
BEAM EFFICIENCY CALCULATIONS (HYBRID METHOD)

The present document has proposed an alternative method (12) to the direct approach (1). A hybrid numerical method may also be employed. Specifically, from (6)

$$\eta_B \approx \frac{\eta_{SO} \iint_{\Omega_0} P_{1_{MP}}(\Omega)\, d\Omega}{\iint_{\Omega_T} (P_{1_{MP}}(\Omega) + P_{1_{CP}}(\Omega))\, d\Omega} \quad , \qquad \text{(1-E)}$$

where $\Omega_T < 4\pi$ is some solid angle to be determined. For symmetric cases, this amounts to selecting some maximum value of the polar angle (θ_T) of a radiation pattern. See Figure E-1. Cross-polarization may be ignored where the contribution is negligible.

As noted previously, separation of the spillover fields and backscattered fields is possible in mathematical simulation, in contrast with physical measurements. This is exploited in the hybrid method also.

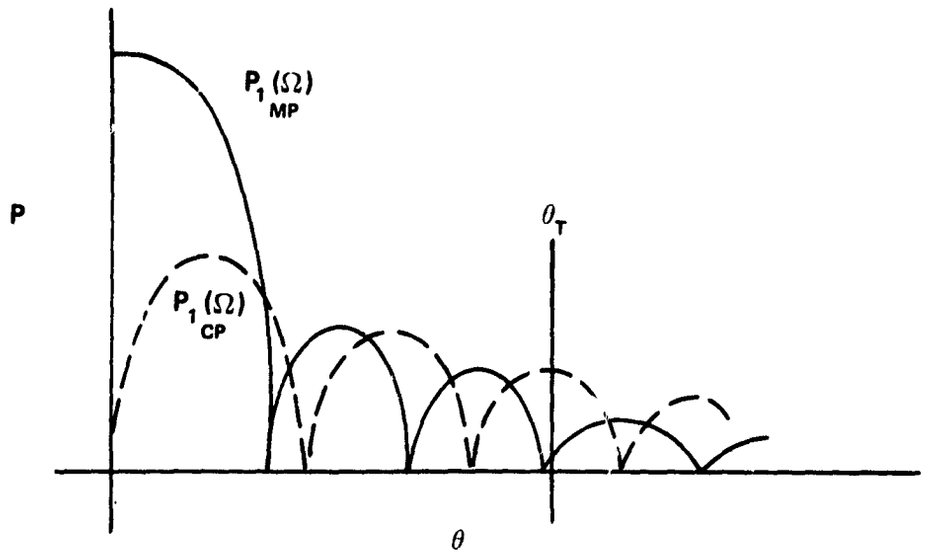

Figure E-1. Truncation of Integration.

Several difficulties are associated with the hybrid method. One of these is that the algorithm which is used to develop the backscattered radiation pattern is often numerical and dependent on some finite sampling (LI) of the complex-vector sheet-current distribution on a reflector surface. For apertures which are electrically large (several hundred wavelengths), the computer cpu-time may establish a limit on (LI), for economic and other practical reasons, so that a spurious radiation pattern will result for the far-out sidelobes. This is illustrated in Figure E-2. More subtle examples exist, for which the sidelobe structure does not descend with fidelity, and an investigator may not always be able to distinguish a spurious result from an accurate simulation. Consequently, there is an element of risk in selection of the truncation angle (θ_T).

Since the illumination distribution is known in a mathematical simulation of the backscattered radiation pattern, it is possible to obtain a satisfactory evaluation of (1-E) by determining the parameters of that distribution and relying on certain analytical results in the literature. Ref. 6, pp. 9-20 to 9-39; Ref. 7, p. 398; Ref. 8, p. 3-22. Equations are available for determining the percentage of power contained in various radiation patterns for any angle θ. In effect, a computed pattern is matched to an analytical example, and an angle θ_T for which most of the

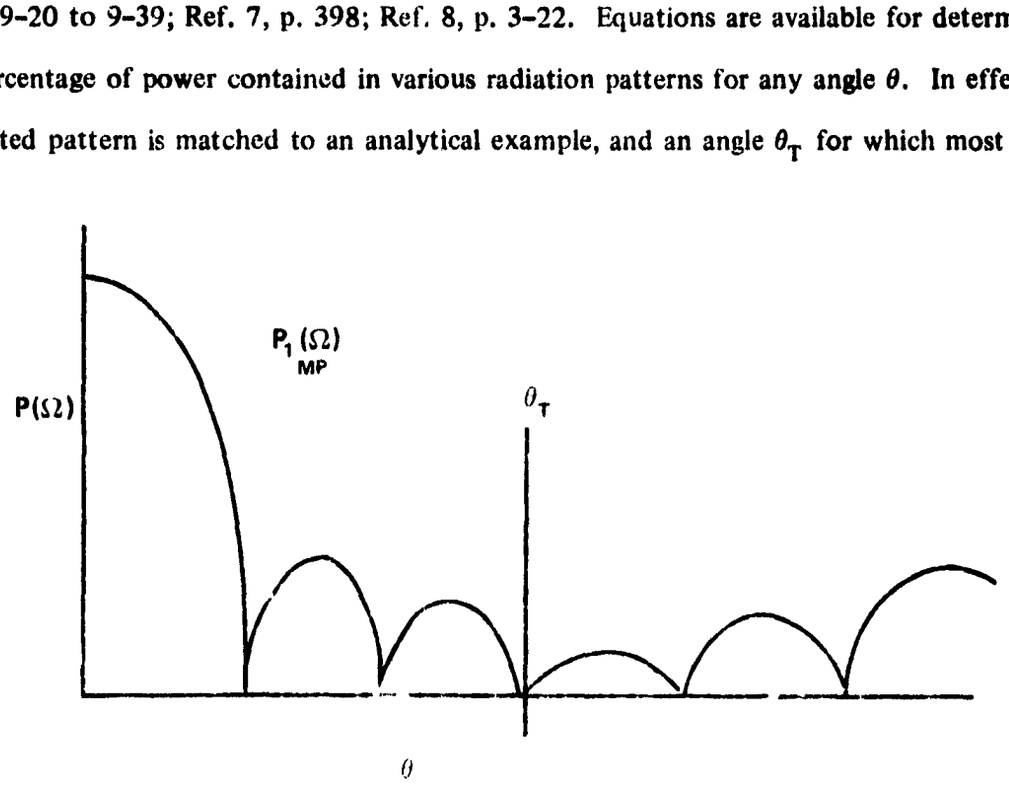

Figure E-2. Spurious Backscatter Calculation.

pattern power is realized is obtained. Often a few sidelobes are sufficient for obtaining 95 per cent or more of the total power.

A small truncation angle (θ_T) can therefore be selected with confidence, avoiding the region of spurious lobes if it exists, and total power can be inferred. Beam efficiency is then obtained as follows, having neglected polarization efficiency here.

$$\eta_B \approx \eta_{SO} \frac{P_{MB}}{(P_{MB} + \sum_{i=1}^{j} P_{SL_i}) + (\sum_{i=j+1}^{k} P_{SL_i})} = \frac{P_{MB}}{P_{TOT.}} \qquad (2\text{-E})$$

where P_{MB} is the main-beam power and P_{SL_i} is the power in the (i^{th}) side-lobe.

The sum of the main beam power and first (j) sidelobe power content can then be obtained by a numerical integration, or by the formula of the matched example. Since the fraction of total power (p) is known at (θ_T), the total power of the radiation pattern is

$$P_{TOT.} = \frac{(P_{MB} + \sum_{i=1}^{j} P_{SL_i})}{p} \quad , \qquad (3\text{-E})$$

so that beam efficiency can be rewritten as

$$\eta_B \approx \eta_{SO} \frac{p\, P_{MB}}{(P_{MB} + \sum_{i=1}^{j} P_{SL_i})} \qquad (4\text{-E})$$

Another difficulty associated with the hybrid method is that the truncation problem may recur for those cases where there is a significant departure from the canonical configurations which exhibit undistorted reflectors, point foci, and idealized feeds with point phase centers which are situated at the classical focal points. For LAMMR, an offset paraboloid will be distorted by a

one-revolution per-second rotation rate of the antenna, and thermal loads in orbit. These distortions will be simulated mathematically, and the radiation patterns and beam efficiency will be recomputed. If a truncation angle (θ_T) which contains a sufficient fraction of the total radiation pattern power (Figure E-3) cannot be assigned with confidence, the alternative method, based on (12) affords a viable alternative. The lack of axial symmetry can be overcome by reverting to numerical integration in two dimensions (θ, ϕ), but the truncation problem appears to compromise the hybrid method.

In conclusion, both the alternative and hybrid methods isolate the spillover factor (η_{SO}), but the alternative method is restricted to the main beam power integration, whereas the hybrid method requires integration out to a truncation angle (θ_T). There is a greater dependence on the algorithm which generates the backscatter pattern when using the hybrid method. Although the alternative method evaluates factors which affect beam efficiency in the aperture before the radiation pattern is formed, this compact approach requires that the subroutines for computing

$$\eta_{POL}\ \eta_A = \eta_{POL}\ \eta_{AM}\ \eta_{AP}$$

be implemented and available.

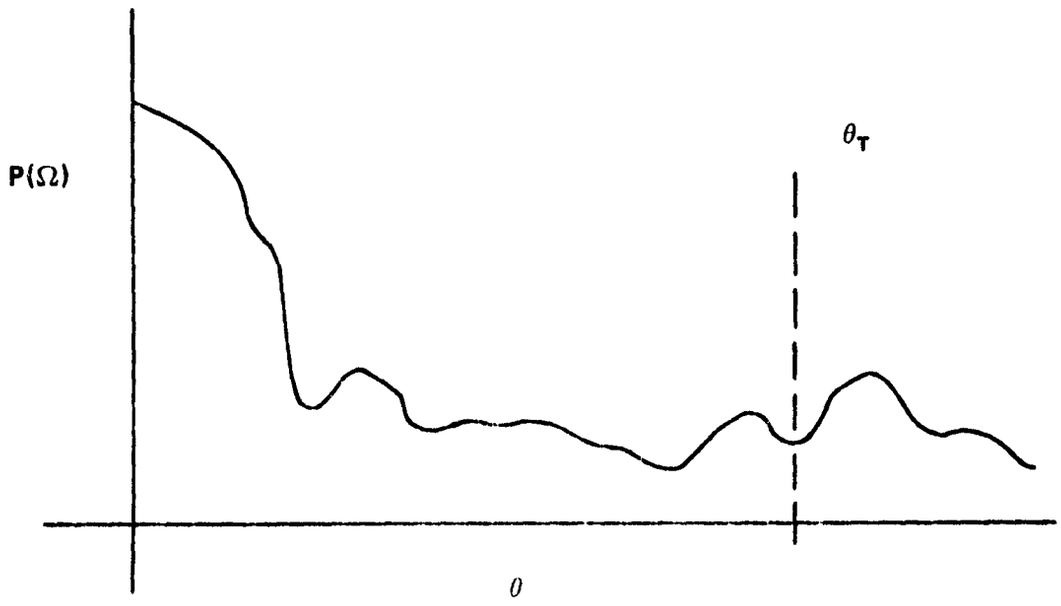

Figure E-3. Arbitrary Truncation.

APPENDIX F
BEAM EFFICIENCY CALCULATIONS (FEED PATTERN METHOD)

A simple means for arriving at beam efficiency is available via equations (4) and (16) of this document. Fujioka has suggested that the feed-power-pattern may used to avoid the difficulties associated with selecting a truncation angle (θ_T) in the hybrid method. Since it has been shown that the spillover fields superimposed on the computed backscattered fields have a total power content formally equal to the sum of the backscattered power plus the spillover power(s), it is possible to reformulate (1) as

$$\eta_B = \frac{\eta_{POL} \iint_{\Omega_0} P_{1_{MP}}(\Omega)\, d\Omega}{\iint_{4\pi} [P_{\mathscr{F}_{MP}}(\Omega) + P_{\mathscr{F}_{CP}}(\Omega)]\, d\Omega} \qquad (1\text{-F})$$

where $P_{\mathscr{F}}(\Omega)$ and $P_{1_{MP}}(\Omega)$ are feed and main-beam power density, respectively.

The approach of equation (1-F) avoids the integration of the sidelobes entirely, and utilizes only the calculated main beam. The integration over $P_{\mathscr{F}}(\Omega)$ is simple, compared to the integration over $P_{1_{MP}}(\Omega)$, $P_{1_{CP}}(\Omega)$ required by the fundamental method, equation (1), since it is a relatively monotonous function. It can be seen that the feed pattern method and the alternative method of this document are similar regarding integration over Ω_0. They differ in that the feed pattern method, while simple to carry out, does not provide the insight or loss budget provided by the collective efficiencies (H) of the alternative method. Polarization efficiency is written explicitly since it depends on the interaction of the incident magnetic vector ($\bar{h}_i$) and the surface normal ($\bar{n}_1$). It may be evaluated over either 4π solid angle in the far field in principle or over the aperture (AP) in practice, as indicated by equation (7).